

A Study on Double Negative Properties of Metal–Dielectric Nanocomposites

REZA GHOLIPUR,¹ ZAHRA KHORSHIDI,¹ and ALI BAHARI^{1,2}

1.—Department of Solid State Physics, University of Mazandaran, 4741695447 Babolsar, Iran.
2.—e-mail: bahari.pa.a@gmail.com

In this paper, we investigate negative permittivity and permeability behaviors of Ag/Zr_{0.9}Ni_{0.1}O_y nanocomposites consisting of Ag nanowires embedded in Ni-doped zirconia (Zr_{0.9}Ni_{0.1}O_y) dielectric. The Ag/Zr_{0.9}Ni_{0.1}O_y nanocomposites with different atomic ratios of Ag were prepared by a co-precipitation process. X-ray diffraction analysis reveals that the silver nanoparticles crystallize in cubic structure with preferred orientation along the [220] direction. Scanning electron microscope studies reveal that grains are prolate spheroid structures and uniformly distributed in the dielectric medium. The experimental data of the negative permittivity are fitted well by the Drude model. The results show that the Ag/Zr_{0.9}Ni_{0.1}O_y nanocomposites enhance double-negative properties. Also, by changing the aspect ratio of Ag, variation of permittivity and permeability changes are introduced.

INTRODUCTION

With the recent resurgence of interest in double-negative (DNG) materials and the reported construction of a metamaterial with DNG characteristics, applications of these materials have become feasible, and the examination of the behavior of systems and devices a potentially fruitful topic.^{1,2}

Double-negative metamaterials (DNMs) refer to artificially patterned metal–dielectric structures having simultaneously negative effective permittivity (ϵ_{eff}) and effective permeability (μ_{eff}).^{3–12} A negative permittivity is not unusual and occurs in any metal from zero frequency to the plasma frequency (ω_p). The plasma oscillation of conduction electrons provided by metal inclusion will be evoked for the near-percolation threshold (p_c) and negative permittivity appears. This implies that the concentration of electrons plays a significant role. It has been proposed that electromagnetic metamaterials composites formed either from periodic or random arrays of scattering elements should respond to electromagnetic radiation as continuous materials.^{13,14}

Fabrication techniques for three-dimensional (3D) ordered metal–dielectric nanostructures include direct electron-beam writing,¹⁵ focused-ion beam chemical vapor deposition,¹⁶ 3D holographic lithography,¹⁷ deep x-ray lithography,¹⁸ and multi-layer nanoimprint lithography.¹⁹ Random or

disordered metal–dielectric composites confined to a thin film can be fabricated by various techniques: thermal evaporation, electron-beam evaporation, and sputtering, as well as by electroplating.²⁰ Random metal–dielectric composites, such as nanoscaled semicontinuous metallic structures, exhibit optical and electrical transport properties that are notably different from those of their corresponding bulk counterparts.^{21–26} The use of metal–dielectric composites is an interesting route to obtain materials with tailorable dielectric and permeability functions. In particular, random metal–dielectric composites are easy to prepare using thin film deposition techniques, and their effective dielectric function can be varied by controlling the mixture composition and particle shape.²⁷ These composites may enable wavelength-tuning of super-resolution devices,²⁸ improve the performance of negative index structures^{29,30} and cloaking devices³¹ and provide transparency or extreme anisotropy.³²

In the present work, we experimentally show that Ag metal nanowires embedded randomly in a Zr_{0.9}Ni_{0.1}O_y dielectric medium can exhibit negative permittivity and permeability at ~8–10 GHz frequencies. For metamaterials at microwave to infrared frequencies, silver is the metal of choice mainly because of its superior (smaller) loss factor compared with other metals. Moreover, a material with

a relatively large dielectric constant is favored for the host dielectric. Therefore, in the present structure, Ni-doped zirconia is used.

EXPERIMENTAL

Dielectric Synthesis

The $Zr_{0.9}Ni_{0.1}O_y$ nanostructural sample was prepared through a co-precipitation technique using NH_4OH solution. Zirconyl chloride octahydrate [$ZrOCl_2 \cdot 8H_2O$] and nickel(II) chloride [$NiCl_2 \cdot 6H_2O$] were used as the dielectric precursors. Aqueous solutions of 1 M concentrations of zirconyl chloride octahydrate and nickel (II) chloride were prepared. NH_4OH solution was added dropwise to a beaker containing a solution with 90 wt.% zirconyl chloride octahydrate and 10 wt.% nickel (II) chloride with stirring by a magnetic stirrer.

Silver Nanoparticles Growth

Silver nanoparticles were synthesized by reducing $AgNO_3$ in ethylene glycol (EG) [$C_2H_6O_2$] and *n,n*-dimethylformamide (DMF) [$C_3H_7O_N$] (EG/DMF). Polyvinyl pyrrolidone (PVP) was introduced as a structure-directing agent. Gold nanoparticles derived by in situ pre-reducing chloroauric acid ($HAuCl_4$) in EG/DMF were used as seeds. Firstly, $HAuCl_4$ solution was prepared from mixing 10 mL of EG/DMF with 1 mL of 0.005 M $HAuCl_4$. A few minutes later, 170 mg of $AgNO_3$ dissolved in 10 mL of EG/DMF and 170 mg PVP dissolved in 10 mL of EG/DMF were added to the $HAuCl_4$ solution with the same injection rate of 2 mL/min. This solution was stirred vigorously at 160°C for 2 h. Silver nanowires began forming at this stage.

The solution was diluted with acetone and centrifuged at 2000 rpm for ~20 min. Ag nanoparticles were dispersed in a Zr and Ni solution with different atomic ratios “[Ag]/[$Zr_{0.9}Ni_{0.1}O_y$] = x ” [where “ x ” is 0 (named Ag_0/ZN sample), 0.03 (named $Ag_{0.03}/ZN$ sample), and 0.12 (named $Ag_{0.12}/ZN$ sample)] under vigorous magnetic stirring. The solution was poured into a plastic dish and sonicated for 60 min.

Analyses of Phase and Morphology

For the crystal and phase analyses, XRD measurements with $Cu K\alpha$ ($\lambda = 1.5408 \text{ \AA}$) radiation by a GBC-MMA007 (2000) instrument were performed. Microscopy analysis and surface morphology were performed using SEM, AFM, and TEM techniques. The SEM images of the films were studied by a XL30-PHILIPS instrument.

The Permittivity and Permeability Measurements

The theories for the permittivity and permeability measurements are the “parallel plate capacitor” and “inductance” methods. The parallel plate capacitor method involves sandwiching material between two electrodes to form a capacitor.

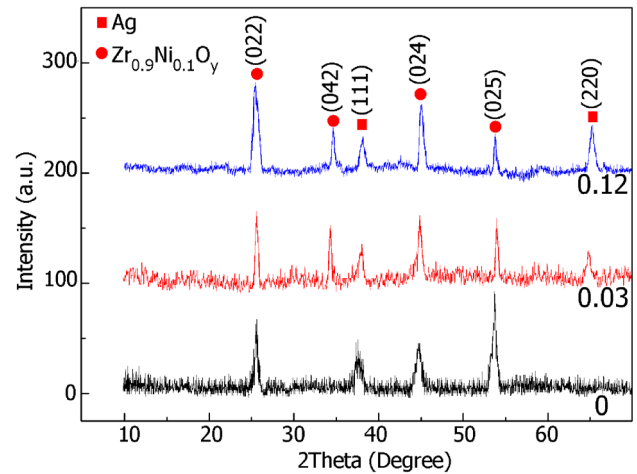


Fig. 1. XRD patterns of the Ag_x/ZN samples ($x = 0, 0.03$ and 0.12).

RESULTS AND DISCUSSION

XRD

Figure 1 shows the XRD patterns of the Ag_x/ZN samples. The XRD data indicated the presence of some diffraction peaks belonging to the two-phase mixture of the cubic phase of Ag and the tetragonal phase of $Zr_{0.9}Ni_{0.1}O_y$. The six main diffraction peaks of $Zr_{0.9}Ni_{0.1}O_y$ and Ag identified with the JCPDS databases (01-081-0610) and (00-001-1164), respectively, are typical of these phases. It was also found that, as the molar silver content increased, the width of the peaks became stronger. Furthermore, the intensities of different diffraction peaks are different, which indicates that the growth of Ag_x/ZN in various planes is different and the growth is anisotropic.

Moreover, the shift of the (042) diffraction peak towards the higher angles is observed when the Ag content increases.

From the XRD spectra, the crystallite size (D) of Ag_x/ZN samples was obtained using the Debye-Scherrer formula, as shown in Eq. 1:³³

$$D = \frac{0.94\lambda}{\beta \cos \theta}, \quad (1)$$

where $\lambda = 1.5408 \text{ \AA}$ and β is the FWHM. It was calculated that, as the molar silver content increased, the average crystallite size of the dielectric nanoparticles became smaller.

Morphology Analyses

The morphology of the Ag_x/ZN samples was observed by SEM images (Fig. 2). For $x = 0$, the sample shows a nano-sized grain structure which decreased when the content of the doping element was increased to 0.03 and 0.12. As Fig. 2a shows, no nanowire was obtained when there was no silver. It was found that the Ag_0/ZN reveals spherical shapes with an average grain size of 70–180 nm, which is

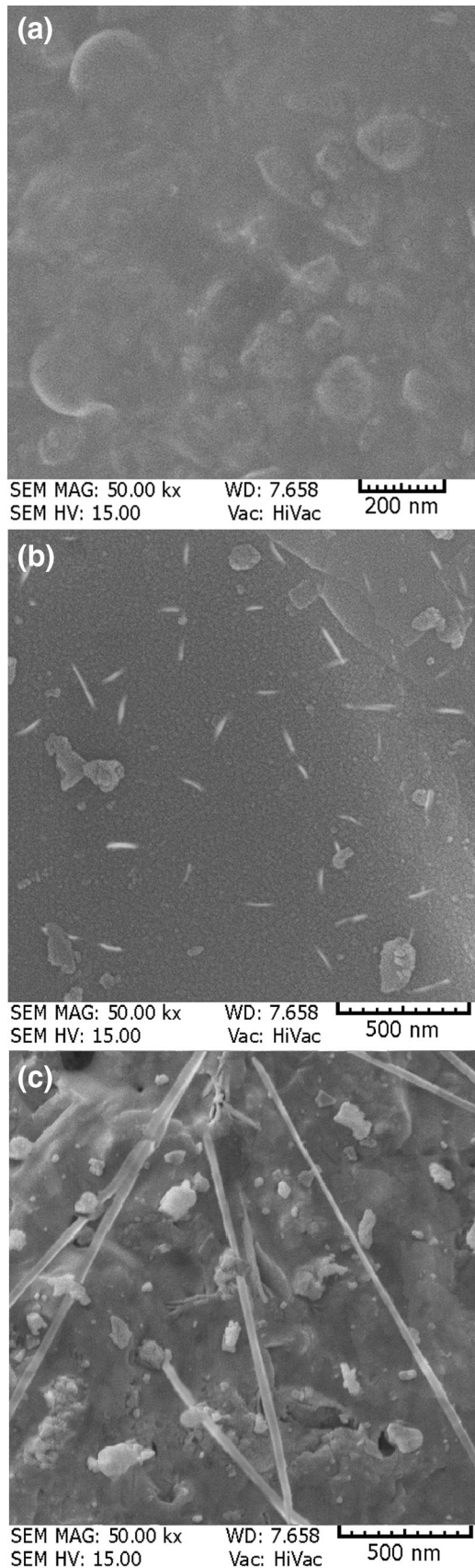


Fig. 2. SEM images of: (a) Ag_0/Zn ; (b) $\text{Ag}_{0.03}/\text{Zn}$; (c) $\text{Ag}_{0.12}/\text{Zn}$ samples.

much larger as compared to the structure sizes observed in the $\text{Ag}_{0.12}/\text{Zn}$ sample. Figure 2b shows randomly oriented and distinct prolate spheroid structures, and grains with a length of about 10–350 nm and diameters of 2–15 nm. As the silver molar content increases, the grains become uniform prolate spheroid structures (nanowires) with lengths of about 11,002,000 nm and diameters of 5–15 nm (Fig. 2c). Figure 2c also shows that the sample surface increases the random distribution of nanowires, coarseness and inhomogeneity with increasing Ag doping.

The Permittivity and Permeability Analyses

The real parts of the effective dielectric constant (ϵ'_e) of Ag_x/Zn nanocomposites are shown in Fig. 3a and b. The real part of ϵ_e for Ag_0/Zn slowly decrease with frequency. ϵ'_e is positive and decreases with increasing frequency because of polarizations of localized electrons and interfacial. Moreover, ϵ'_e increases with higher silver content because of the increase in the $\text{Ag-Zr}_{0.9}\text{Ni}_{0.1}\text{O}_y$ interface area. By increasing the Ag content, the effect of Ag particles on the dielectric behavior of the composites becomes remarkable. Interestingly, the ϵ'_e turns negative when the silver content reaches 12 wt.% (above p_c). The negative ϵ'_e implies the absence of polarization generated by the dielectric.

The behavior of the ϵ'_e of $\text{Ag}_{0.12}/\text{Zn}$ sample is well fitted by the frequency dispersion formula of the modified Drude theory as follows:

$$\epsilon'_e = 1.00 - \frac{438.2}{\left(\frac{\nu}{1\text{E}10}\right)^2 + \left(\frac{1100}{1\text{E}4}\right)^2}; \quad \text{for } \text{Ag}_{0.12}/\text{Zn}, \quad (2)$$

where ν is frequency. For the $\text{Ag}_{0.12}/\text{Zn}$ sample, the ϵ'_e has a metallic-like behavior and its sign is negative when $\omega < \omega_p$ (plasma frequency). According to formula 2, ω_p are damping constants (Γ) of about 1.313 THz and 6.911 GHz, respectively. This equation gives a dispersion behavior of the effective dielectric constant ϵ'_e .

Figure 3c and d presents the dependence of the imaginary parts of the effective dielectric constant (ϵ''_e) of the Ag_x/Zn samples on frequency. As shown in Fig. 3c and d, ϵ''_e is dependent on the whole measured frequency range for the Ag_x/Zn samples. As for the Ag_0/Zn and $\text{Ag}_{0.03}/\text{Zn}$ samples (below p_c), ϵ''_e shows a slight slope with increasing frequency because of increasing dielectric loss and leakage conductance loss. When the Ag content reaches the value of 0.12 (above p_c), ϵ''_e reduces rapidly with frequency, e.g., from 0.5 GHz to 1 GHz. In comparison with our previous results,² the results presented in this study show that Ag nanowires synthesized with more aspect ratio have more negative permittivity and permeability.

Figure 4a shows the frequency dependence of real parts of the effective permeability (μ'_e) for the Ag_x/Zn samples. The encapsulation of Ag nanowires

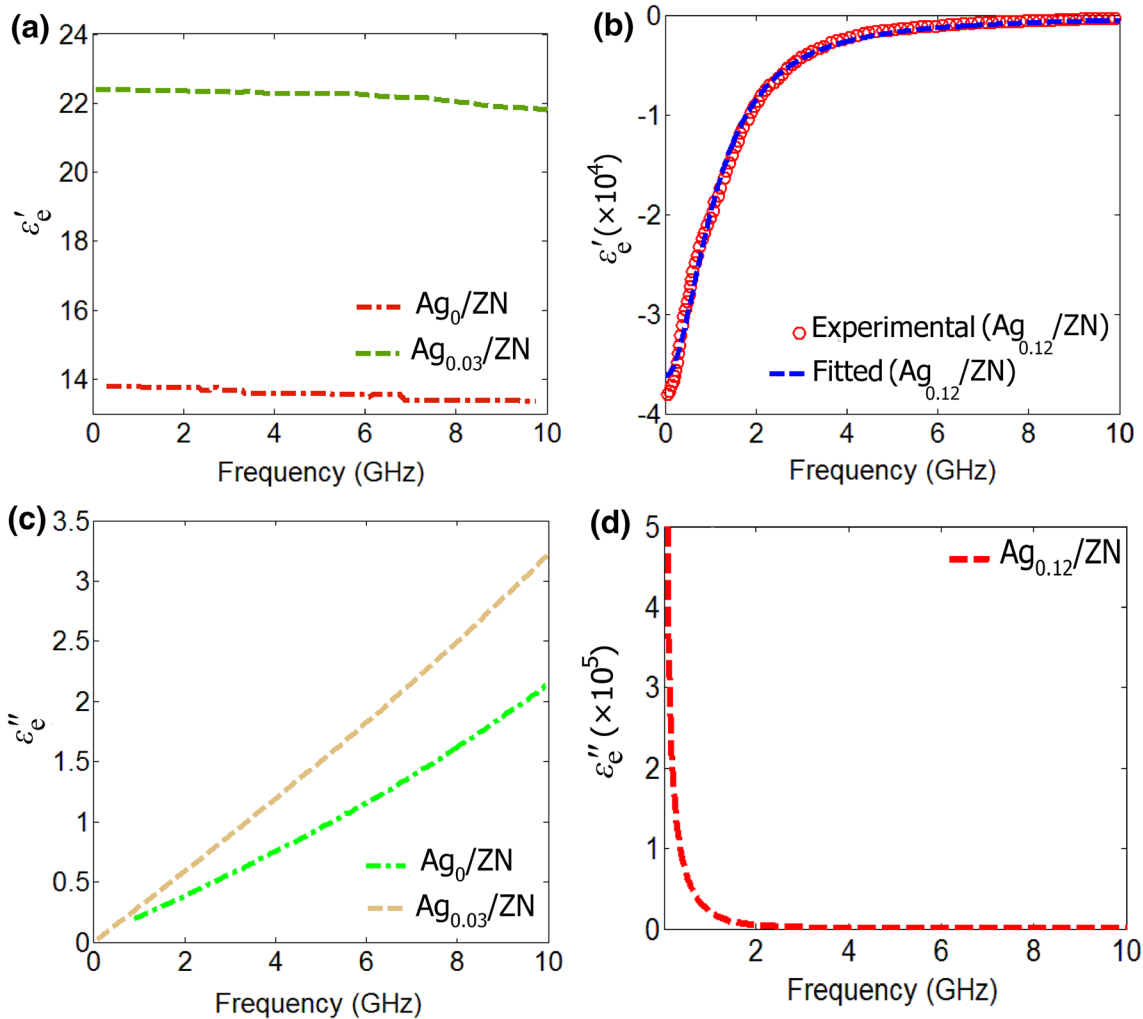


Fig. 3. Frequency dependence of (a and b) real parts and fitted results; (c and d) imaginary parts of the effective dielectric constant for Ag_x/Zn samples.

with $\text{Zr}_{0.9}\text{Ni}_{0.1}\text{O}_y$ results in the enhancement of the magnetic property resulting from the $\text{Zr}_{0.9}\text{Ni}_{0.1}\text{O}_y$ magnetic resonance and the increased inductance and capacitance. It is worth pointing out that the μ_e' of $\text{Ag}_{0.12}/\text{Zn}$ is smaller than the μ_e' of the $\text{Ag}_{0.03}/\text{Zn}$ sample, which can be attributed to the topology of the $\text{Ag}_{0.12}/\text{Zn}$ sample. It is clear that the $\text{Ag}_{0.12}/\text{Zn}$ sample with the geometry of randomly oriented nanowires has caused a rise of the low inductance and capacitance and hence a decline in the magnetic response in the test frequency range inside the $\text{Ag}_{0.12}/\text{Zn}$ composite. Hence, the μ_e' can be considered low in the frequency range.

In the high-frequency range, because of eddy currents and Lenz's law, the real part of the magnetic permeability becomes smaller than zero, and the diamagnetic behavior for $\text{Ag}_{0.12}/\text{Zn}$ sample appears near the frequency of 8 GHz.

The domain wall motion and gyromagnetic spin resonances of the dielectric medium contribute to the negative μ_e' phenomenon and the continuous

decrease of μ_e' with increasing frequency. The $\text{Ag}_{0.12}/\text{Zn}$ sample has negative responses at some frequencies. The reason for such behavior is the collective response of the wired-like network structure and the dielectric medium to the electromagnetic field.

Plots of imaginary parts of the effective magnetic permeability (μ_e'') versus frequency for the Ag_x/Zn samples are shown in Fig. 4b. The μ_e'' decrease in the high-frequency range as the Ag content increases. The frequency at the maximum of the μ_e'' decreases on its approach to the 3 wt.% Ag.

Electrical Analyses

The frequency responses of reactance Z'' for the Ag_x/Zn samples are shown in Fig. 5. It can be seen that, for the Ag_0/Zn and $\text{Ag}_{0.03}/\text{Zn}$ samples, the signs of reactance are negative, which manifests its capacitive character, and, for the $\text{Ag}_{0.12}/\text{Zn}$ sample, the sign of reactance is positive, which manifests its inductive character.

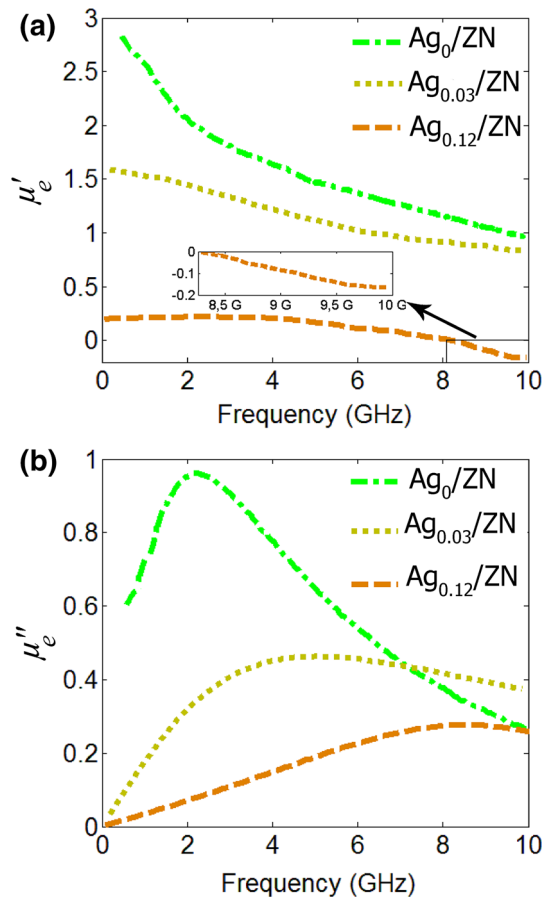


Fig. 4. Plots of (a) real parts; (b) imaginary parts of the effective magnetic permeability for Ag_x/Zn samples.

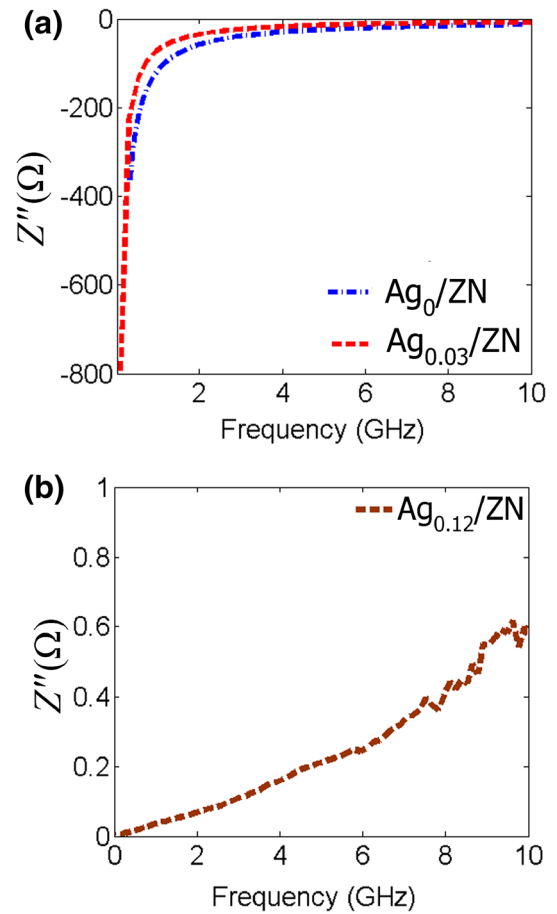


Fig. 5. Frequency dependence of reactance for Ag_x/Zn samples (a) $x = 0$ and 0.03 ; (b) $x = 0.12$.

CONCLUSION

We have discussed the preparation process and the morphological, electrical, magnetic and optical properties of $\text{Ag}/\text{Zr}_{0.9}\text{Ni}_{0.1}\text{O}_y$ nanocomposites at microwave frequencies. By increasing the Ag molar content elongated nanoparticles were uniformly distributed. The effective magnetic properties are due to the magnetic resonance and eddy current of the samples with an external magnetic field. The effective plasma frequency of $\text{Ag}_{0.12}/\text{Zn}$ is much lower than that of the plasma frequency of bulk silver ($\omega_p = 2.18\text{E}15$) due to a dilution of the effective electron concentration and a considerable increase of m_e . The effective properties of this nanocomposite have been shown to be useful for DNMs at this range of frequencies. Our results may be very helpful to better understand the dielectric properties of nanocomposites in the microwave frequency region and to optimize device parameters in the future. The outcome is negative ϵ_e' and μ_e' for $\text{Ag}_{0.12}/\text{Zn}$. The tunability negative permittivity and permeability makes $\text{Ag}_{0.12}/\text{Zn}$ a promising candidate for DNMs.

REFERENCES

1. R. Stanley, Williams. *JOM* 59, 58 (2007).
2. R. Gholipur and A. Bahari, *Opt. Mater.* 50, 175 (2015).
3. W. Zhu, X. Zhao, B. Gong, L. Liu, and B. Su, *Appl. Phys. A* 112, 147 (2010).
4. S. Linden, C. Enkrich, M. Wegener, J.F. Zhou, T. Koschny, and C.M. Soukoulis, *Science* 306, 1351 (2004).
5. W.S. Cai, U.K. Chettiar, H.K. Yuan, V.C. de Silva, A.V. Kildishev, V.P. Drachev, and V.M. Shalaev, *Opt. Express* 15, 3333 (2007).
6. V.M. Shalaev, W.S. Cai, U.K. Chettiar, H.K. Yuan, A.K. Sarychev, V.P. Drachev, and A.V. Kildishev, *Opt. Lett.* 30, 3356 (2005).
7. S. Zhang, W.J. Fan, N.C. Panoiu, K.J. Malloy, R.M. Osgood, and S.R.J. Brueck, *Phys. Rev. Lett.* 95, 137404 (2005).
8. G. Dolling, C. Enkrich, M. Wegener, C.M. Soukoulis, and S. Linden, *Science* 312, 892 (2006).
9. G. Dolling, M. Wegener, C.M. Soukoulis, and S. Linden, *Opt. Lett.* 32, 53 (2007).
10. U.K. Chettiar, A.V. Kildishev, H.K. Yuan, W.S. Cai, S.M. Xiao, V.P. Drachev, and V.M. Shalaev, *Opt. Lett.* 32, 1671 (2007).
11. E. Plum, V.A. Fedotov, A.S. Schwanecke, N.I. Zheludev, and Y. Chen, *Appl. Phys. Lett.* 90, 223113 (2007).
12. M. Decker, M.W. Klein, M. Wegener, and S. Linden, *Opt. Lett.* 32, 856 (2007).
13. J.B. Pendry, A.J. Holden, W.J. Stewart, and I. Youngs, *Phys. Rev. Lett.* 76, 4773 (1996).

14. J.B. Pendry, A.J. Holden, D.J. Robbins, and W.J. Stewart, *IEEE Trans. Microw. Theory Technol.* 47, 2075 (1999).
15. S. Griffith, M. Mondol, D.S. Kong, and J.M. Jacobson, *J. Vac. Sci. Technol. B* 20, 2768 (2002).
16. T. Morita, K. Kondo, T. Hoshino, T. Kaito, J. Fujita, T. Ichihashi, M. Ishida, Y. Ochiai, T. Tajima, and S. Matsui, *J. Vac. Sci. Technol. B* 22, 3137 (2004).
17. M. Campbell, D.N. Sharp, M.T. Harrison, R.G. Denning, and A.J. Turberfield, *Nature* 404, 53 (2000).
18. W. Ehrfeld and H. Lehr, *Radiat. Phys. Chem.* 45, 349 (1995).
19. N. Kehagias, V. Reboud, G. Chansin, M. Zelsmann, C. Jeppesen, C. Schuster, M. Kubenz, F. Reuther, G. Gruetzner, and C.M.S. Torres, *Nanotechnology* 18, 175303 (2007).
20. R. Gholipur and A. Bahari, *Mater. Des.* 94, 139 (2016).
21. J.B. Pendry, L. Martin-Moreno, and F.J. Garcia-Vidal, *Science* 305, 847 (2004).
22. A.V. Krasavin, K.F. MacDonald, A.S. Schwanecke, and N.I. Zheludev, *Appl. Phys. Lett.* 89, 031118 (2006).
23. T. Kume, T. Amano, S. Hayashi, and K. Yamamoto, *Thin Solid Films* 264, 115 (1995).
24. A.K. Sarychev and V.M. Shalaev, *Phys. Rep.* 335, 276 (2000).
25. V.A. Shubin, A.K. Sarychev, J.P. Clerc, and V.M. Shalaev, *Phys. Rev. B* 62, 11230 (2000).
26. R. Gholipur and A. Bahari, *Opt. Quantum Electron.* 48, 37 (2016).
27. L. Shi, L. Gao, S. He, and B. Li, *Phys. Rev. B* 76, 045116 (2007).
28. Y. Xiong, Z.W. Liu, S. Durant, H. Lee, C. Sun, and X. Zhang, *Opt. Express* 15, 7095 (2007).
29. U.K. Chettiar, A.V. Kildishev, T.A. Klar, and V.M. Shalaev, *Opt. Express* 14, 7872 (2006).
30. L. Menon, W.T. Lu, A.L. Friedman, S.P. Bennett, D. Heiman, and S. Sridhar, *Appl. Phys. Lett.* 93, 123117 (2008).
31. W. Cai, U.K. Chettiar, A.V. Kildishev, and V.M. Shalaev, *Nat. Photonics* 1, 224 (2007).
32. J.S. Parramon, V. Janicki, and H. Zorc, *Opt. Express* 18, 26915 (2010).
33. G.E.M. Jauncey and F. Pennell, *Phys. Rev. B* 43, 505 (1993).